Saudi Pharmaceutical Journal 28 (2020) 290–299

Contents lists available at ScienceDirect

Saudi Pharmaceutical Journal

journal homepage: www.sciencedirect.com

Original article

Bioresorbable hydrogels prepared by photo-initiated crosslinking of diacrylated PTMC-PEG-PTMC triblock copolymers as potential carrier of antitumor drugs

Yuandou Wang [a], Laishun Xi [b], Baogang Zhang [a], Qingzhen Zhu [b], Feng Su [a,b,*], Katarzyna Jelonek [c,*], Arkadiusz Orchel [d], Janusz Kasperczyk [c,d], Suming Li [e,*]

[a] Institute of High Performance Polymers, Qingdao University of Science and Technology, Qingdao 266042, China
[b] State Key Laboratory Base of Eco-chemical Engineering, College of Chemical Engineering, Qingdao University of Science and Technology, Qingdao 266042, China
[c] Centre of Polymer and Carbon Materials, Polish Academy of Sciences, Curie-Sklodowska 34 St., 41-819 Zabrze, Poland
[d] Medical University of Silesia, School of Pharmacy with the Division of Laboratory Medicine in Sosnowiec, Department of Biopharmacy, 8 Jedności Str., 41-200 Sosnowiec, Poland
[e] Institut Europeen des Membranes, UMR CNRS 5635, Universite de Montpellier, 34095 Montpellier, France

ARTICLE INFO

Article history:
Received 23 October 2019
Accepted 26 January 2020
Available online 31 January 2020

Keywords:
Bioresorbable
Hydrogels
Poly(trimethylene carbonate)
Drug release
Doxorubicin
Biocompatibility
Cyto-toxicity

ABSTRACT

PTMC-PEG-PTMC triblock copolymers were prepared by ring-opening polymerization of trimethylene carbonate (TMC) in the presence of dihydroxylated poly(ethylene glycol) (PEG) with Mn of 6000 and 10,000 as macro-initiator. The copolymers with different PTMC block Lengths and the two PEGs were end functionalized with acryloyl chloride. The resulting diacrylated PEG-PTMC-DA and PEG-DA were characterized by using NMR, GPC and DSC. The degree of substitution of end groups varied from 50.0 to 65.1%. Hydrogels were prepared by photo-crosslinking PEG-PTMC-DA and PEG-DA in aqueous solution using a water soluble photo-initiator under visible light irradiation. The effects of PTMC and PEG block lengths and degree of substitution on the swelling and weight loss of hydrogels were determined. Higher degree of substitution leads to higher crosslinking density, and thus to lower degree of swelling and weight loss. Similarly, higher PTMC block length also leads to lower degree of swelling and weight loss. Freeze dried hydrogels exhibit a highly porous structure with pore sizes from 20 to 100 μm.

The biocompatibility of hydrogels was evaluated by MTT assay, hemolysis test, and dynamic clotting time measurements. Results show that the various hydrogels present outstanding cyto- and hemo-compatibility. Doxorubicin was taken as a model drug to evaluate the potential of PEG-PTMC-DA and PEG-DA hydrogels as drug carrier. An initial burst release was observed in all cases, followed by slower release up to more than 90%. The release rate is strongly dependent on the degree of swelling. The higher the degree of swelling, the faster the release rate. Finally, the effect of drug loaded hydrogels on SKBR-3 tumor cells was evaluated in comparison with free drug. Similar cyto-toxicity was obtained for drug loaded hydrogels and free drug at comparable drug concentrations. Therefore, injectable PEG-PTMC-DA hydrogels with outstanding biocompatibility and drug release properties could be most promising as bioresorbable carrier of hydrophilic drugs.

1. Introduction

Cancer is one of the most common causes of death of the humanity. Chemotherapy is applied after surgical treatment of most cancers (Bhosle and Hall, 2009; Saberzadeh-Ardestani et al., 2019). However, clinically used anticancer drugs present systemic toxicity and strong side effects on normal tissues and organs. Doxorubicin (DOX), an anthracycline antibiotic, is an efficient chemotherapeutic drug which has been used in clinics for over forty years. The potential side effects that can cause multi-organ toxicities especially cardiotoxicity have to be taken into

* Corresponding authors at: Institut Europeen des Membranes, UMR CNRS 5635, Universite de Montpellier, 34095 Montpellier, France (S. Li).
E-mail addresses: sufeng@qust.edu.cn (F. Su), kjelonek@cmpw-pan.edu.pl (K. Jelonek), suming.li@umontpellier.fr (S. Li).

Peer review under responsibility of King Saud University.

Production and hosting by Elsevier

https://doi.org/10.1016/j.jsps.2020.01.008
1319-0164/

consideration for systemic medication (Altieri et al., 2016; Yang et al., 2017; Pugazhendhi et al., 2018).

Topical treatment of cancers presents great interest as it allows to ensure adequate drug dose in the lesion and to reduce the side effects related to systemic medication. Various novel drug delivery carriers have been investigated, including hydrogels (Oh et al., 2019; Ullah et al., 2019; Ullah et al., 2019), micelles (Su et al., 2019; Liu et al., 2018), nanoparticles (Liyanage et al., 2019), nanogels (Qureshi and Khatoon, 2019), liposomes (Kavian et al., 2019; Cheng et al., 2019), etc.

Hydrogels are a three dimensional network formed by hydrophilic or amphiphilic polymers via physical or chemical crosslinking, and thus are capable of absorbing large amount of water without dissolution. Since the pioneering research by Wichterle and Lim. dating back to 1960 (Wichterle and Lim, 1960), hydrogels have been widely investigated for biomedical and pharmaceutical applications in drug delivery (Schneider et al., 2016; Kim et al., 2019; Ross et al., 2019), tissue engineering (Buchtova et al., 2018; Echave et al., 2019), cell scaffold (Brunelle et al., 2018; Whitely et al., 2018) and wound dressing (Koehler et al., 2018; Hamedi et al., 2018). In particular, injectable hydrogels can achieve high drug concentration and sustained drug release at the target site, which well complies with the requirements of topical treatment (Bastiancich et al., 2019; Tomić et al., 2019; Zhang et al., 2018). Meanwhile, drug delivery by injection allows to effectively reduce the pain and cost related to invasive surgery.

In the past decades, a great deal of research has focused on drug delivery systems prepared from amphiphilic block copolymers composed of a hydrophilic block such as poly(ethylene glycol) (PEG), and a degradable and hydrophobic polyester block such as polylactide (PLA), polyglycolide (PGA), poly(ε-caprolactone) (PCL) and poly(trimethylene carbonate) (PTMC). These copolymers are most promising as drug carrier as they are able to form hydrogels by crosslinking, or nano-sized aggregates by self-assembly. PTMC is an amorphous polycarbonate with a glass transition at −12 °C (Wang et al., 2016). It is thus an elastomeric material at room temperature, and has been used as a softening component in biodegradable copolymer sutures such as Maxon® and Biosyn®. In contrast to polyesters, no acidic species are produced during degradation of PTMC (Wang et al., 2018; Xi et al., 2019).

Zhang et al. reported hydrogels prepared by photo-crosslinking acrylate functionalized PTMC–PEG-PTMC copolymers (Zhang et al., 2009; Zhang et al., 2011). The resulting hydrogels exhibited low elastic modulus and high toughness, and were used as cell scaffold by culturing mesenchyme stem cells and bovine chondrocytes for cartilage tissue engineering. Sharifi et al. investigated PTMC–PEG-PTMC copolymers as an injectable macromer which solidifies in situ upon illumination with visible light (Sharifi et al., 2011). The potential of the materials to seal an opening in the annulus fibrosus was evaluated. The authors also reported nanocomposite hydrogels prepared from PTMC-PEG-PTMC and clay nanoparticles (Sharifi et al., 2012). However, little research has been done on the potential of PTMC–PEG-PTMC hydrogels as carrier of antitumor drugs, so far.

Biocompatibility is a prerequisite for use of a biomaterial in the body's tissues and organs. Ideally, gel formation proceeds in aqueous medium, wherein bioactive agents or cells are dissolved or suspended. Reaction involving high temperature, toxic crosslinkers such as hexamethylene isocyanate or glutaraldehyde should be avoided. Therefore, photo-initiation that generates free radicals upon exposure to light is a method of choice due to mild reaction conditions. Lithium phenyl-2,4,6- trimethylbenzoylphosphinate (LAP) has been used as water soluble type I photo-initiator to prepare PEG diacrylate hydrogels with encapsulation of cells (Majima et al., 1991; Fairbanks et al., 2009). Gelation is achieved under visible light irradiation, in contrast to ultraviolet light used in the case of I2595 as photo-initiator.

In this study, a series of PTMC-PEG-PTMC triblock copolymers were synthesized by ring-opening polymerization of TMC in the presence of PEG with Mn of 6 K and 10 K g/mol, using low toxic stannous octoate as catalyst. Acrylation of both ends of copolymer chains was realized using acryloyl chloride. PTMC-PEG-PTMC diacrylate hydrogels were prepared through photo-crosslinking using LAP as photo-initiator. The chemical structure, swelling ratio and weight loss of hydrogels were determined. *In vitro* biocompatibility of hydrogels was evaluated from the aspects of cytocompatibility and hemocompatibility. Meanwhile, drug loading and drug release behaviors of the hydrogels with various compositions were investigated using doxorubicin (DOX) as a hydrophilic model drug. The effect of drug loaded hydrogels on proliferation of tumor cells was evaluated *in vitro* by sulforhodamine B (SRB) assay.

2. Materials and methods

2.1. Materials

PEG with Mn of 6 K and of 10 K g/mol was obtained from Sigma-Aldrich (USA), and vacuum dried at 60 °C overnight to remove residual water before use. Stannous octoate, trimethylamine (TEA), DOX, acryloyl chloride, dichloromethane, dimethyl phenylphosphonite, 2,4,6-trimethylbenzoly chloride, lithium bromide, and 2-butanone were purchased from Aladdin (China), and used as received. Diethyl carbonate, 1,3-propanediol, dimethylbenzene, dibutyltin dilaurate, zinc powder and sodium metal were supplied by Sinopharm Chemical Reagent Co., Ltd (Shanghai, China). SK-BR-3 and L929 cells were purchased from ATCC (USA). Fetal bovine serum (FBS), pH 7.4 phosphate-buffered saline (PBS), MoCoy 5A and DMEM with penicillin and streptomycin were obtained from Gibco (USA). Transwell with PC membrane was purchased from Corning (USA).

2.2. Synthesis of polymers

TMC was prepared according to the procedure reported in literature (Dong et al., 2014). Typically, 152 g 1,3-propanediol, 248 g diethyl carbonate, 100 mL dimethylbenzene, 0.2 g dibutyltin dilaurate and 0.02 g sodium metal were refluxed at 145 °C for 6 h. Excessive dimethylbenzene and unreacted diethyl carbonate were eliminated by distillation. Thermal decomposition and cyclization then proceeded at 180 °C for 12 h using zinc powder as catalyst. The crude product was purified five times by recrystallization from a mixture of acetone/ethyl ether (v/v = 1/3), followed by vacuum drying at room temperature for 72 h.

PTMC-PEG-PTMC triblock copolymers were synthesized by ring opening polymerization of TMC, using PEG as macro-initiator and $Sn(Oct)_2$ as catalyst as previously described (Yang et al., 2007). Briefly, predetermined amounts of PEG, TMC and $Sn(Oct)_2$ were transferred into a dried flask, and degassed. Polymerization then proceeded at 130 °C for 3 days under N_2 atmosphere. The crude products were dissolved in dichloromethane, precipitated in cold diethyl ether, and then vacuum dried at 60 °C up to constant weight.

Acrylation of the hydroxyl endgroups of PTMC-PEG-PTMC triblock copolymers was realized by esterification using acryloyl chloride. The copolymer was dissolved in dichloromethane under N_2 atmosphere. TEA was added under stirring for 30 min in an ice bath. Acryloyl chloride in dichloromethane was then added to the mixture dropwise. The molar ratio of the hydroxyl endgroup/

TEA/acryloyl chloride was set at 1:2:2. The reaction first proceeded in an ice bath for 30 min, and then at 40 °C for 24 h under N_2 protection. The reaction mixture was cooled down to room temperature, and precipitated in cold diethyl ether. The precipitates were vacuum dried for 3 days after filtration, dissolved in deionized water, dialyzed against deionized water over 3 days, and finally lyophilized to yield a diacrylated copolymer, PEG-PTMC-DA. PEG-DA was synthesized from PEG and acryloyl chloride under similar conditions.

2.3. Synthesis of photo-initiator

Dimethyl phenylphosphonite (0.01 mmol) was added to a three-neck flask under N_2 atmosphere at room temperature. 2,4,6-Trimethylbenzoyl chloride (0.01 mmol) was added dropwise to the flask under continuous stirring. The reaction mixture was stirred for 24 h. Lithium bromide (0.04 mmol) in 60 mL 2-butanone was then added, and the reaction mixture was heated to 50 °C. After 10 min, a solid precipitate was obtained. The mixture was cooled down to ambient temperature, kept for 4 h, and then filtered. The filtrate was washed 3 times with 2-butanone to remove unreacted lithium bromide, and vacuum dried for 3 days to yield LAP in the form of a white powder.

2.4. Preparation of hydrogels

PEG-PTMC-DA hydrogels were prepared by photo-crosslinking using LAP as water-soluble initiator. LAP (0.1 w/v%) and end-functionalized PEG-PTMC-DA or PEG-DA polymers (30 w/v%) were separately dissolved in deionized water. 0.5 mL of each solution was added in a flask and homogenized. The mixed solution was centrifuged at 3000 rpm for 5 min to remove bubbles, and then exposed to visible light (405 nm, 3 W) for 2 min to yield photo-crosslinked PEG-PTMC-DA or PEG-DA hydrogels.

2.5. Characterization

Proton nuclear magnetic resonance (^{1}H NMR) spectra were recorded at room temperature using on a Bruker AVANCE 500 spectrometer (Billerica, USA) operating at 500 MHz. Chemical shifts (δ) were given in ppm using tetramethylsilane as internal reference. $CDCl_3$ and D_2O were used as solvent.

Gel permeation chromatography (GPC) was carried out on a Shimadzu apparatus (Kyoto, Japan) equipped with a Waters 410 refractometer, using tetrahydrofuran (THF) as the mobile phase at a flow rate of 1.0 mL/min. The sample concentration was 1.0 mg/mL, and polystyrene standards were used for calibration.

Differential scanning calorimetry (DSC) was performed using a DSC10 instrument (TA Instruments, USA). Samples of *c.a* 5.0 mg were heated from 25 to 100 °C at a rate of 10 °C/min to determine the melting temperature (T_m) of polymers.

The degree of swelling and weight loss of hydrogels were determined to evaluate their stability in aqueous media. Predetermined amount (W_0) of PEG-PTMC-DA or PEG-DA copolymer was photo-crosslinked to yield a hydrogel sample as described above. The samples were immersed in pH 7.4 phosphate buffered saline (PBS) at 37 °C. 0.02% w/v NaN_3 was added to the medium to prevent bacterial growth. Samples were taken out after 48 h, gently wiped with filter paper, and weighed to obtain the wet weight (W_1). Subsequently, the samples were lyophilized and weighed again to obtain the dry weight (W_2). The degree of swelling and degree of weight loss were calculated using the following equations:

$$\text{Swelling}(\%) = \frac{W_1 - W_2}{W_2} \times 100\% \quad (1)$$

$$\text{Weight loss}(\%) = \frac{W_0 - W_2}{W_0} \times 100\% \quad (2)$$

The morphology of freeze dried hydrogels was visualized by scanning electron microscopy (VEGA3 TESCAN, Czech Republic) operating with an accelerating voltage of 20 kV. The samples were quenched in liquid nitrogen, carefully fractured, and gold-coated by sputtering before measurements.

2.6. In vitro biocompatibility

2.6.1. MTT assay

L929 cells were used to assess the cytotoxicity of hydrogels. Extracts of freeze dried hydrogels were obtained by soaking the samples in PBS at 0.5–5.0 mg/mL for 72 h. L929 cells in logarithmic growth phase were harvested and diluted to a density of 5×10^4 cells/mL with DMEM culture medium supplemented with 10% FBS, 100 U/mL penicillin and 100 μg/mL streptomycin. 100 μL cell suspension was distributed in each well of a 96-well plate, and incubated for 24 h at 37 °C in a humidified atmosphere containing 5% CO_2. 100 μL extracts of freeze dried hydrogel were then added in each well. After 24, 48 and 72 h, the medium was replaced with DMEM and 3-(4,5-dimethyl-2-thiazolyl)-2,5-diphenyltetrazolium bromide (MTT). After 4 h incubation, the liquid was removed and DMSO was added. The optical density (OD) was measured by using a microplate reader (Elx800, BioTek, USA) after 10 min shaking. All measurements were made in triplicate. The culture medium and a 0.5% aqueous solution of phenol were used as the negative control and positive control, respectively. The cell relative growth ratio (RGR) was calculated from the OD values of the test sample and the negative control according to the following equation:

$$\text{RGR}(\%) = \frac{OD_{test\ \ sample}}{OD_{negatie\ \ control}} \times 100\% \quad (3)$$

The cytotoxicity is noted in 0–5 levels according to the RGR value. Level 0 corresponds to a RGR value above 100, level 1 to 75–99, level 2 to 50–74, level 3 to 25–49, level 4 to 1–24, and level 5 to RGR of 0.

2.6.2. Hemolysis test

Fresh blood was collected from the heart of four weeks old New Zealand rabbit, anti-coagulated (blood: 3.8% sodium citrate = 9:1), and diluted with 0.9% physiological saline (blood: saline = 4:5, v/v) for hemolysis test.

Hemolysis test was performed as described previously (Su et al., 2018). 10 mL extract at 1.0 mg/mL was added into a silanized beaker, and thermostated in a 37 °C water bath for 30 min. 0.2 mL diluted rabbit acid-citrate-dextrose (ACD) was then added. After 60 min, the solution was centrifuged at 2500 rpm for 5 min. The OD value of the supernatant was then measured at 540 nm. Physiological saline and distilled water were used as negative and positive controls, respectively. The hemolytic ratio (HR) was calculated from the OD data of the test sample, negative control and positive control using the following equation:

$$\text{HR}(\%) = \frac{OD_{test\ \ sample} - OD_{negative\ \ control}}{OD_{positive\ \ control} - OD_{negatie\ \ control}} \times 100\% \quad (4)$$

2.6.3. Dynamic clotting time

The dynamic clotting time was measured using the method described previously (Zhang et al., 2010). 25 μL extract of freeze-dried hydrogel containing 0.025 M $CaCl_2$ was added in a siliconized tube, and thermostated at 37 °C for 5 min. Then, 200 μL ACD was added to the tube and homogenized. After pre-determined time intervals, 20 mL distilled water was slowly added to the tube. The OD value of the supernatant was determined using a

microplate reader at 490 nm wavelength. The relative clotting time of each sample was determined from the OD value versus time plots. Experiments were performed in triplicate. Glass tube and siliconized tube were used as positive and negative controls, respectively.

2.7. In vitro drug release

DOX release from PEG-PTMC-DA and PEG-DA hydrogels was realized under *in vitro* conditions. Briefly, 50 mg dried hydrogel was immersed in DOX solution at 5.0 mg/mL, and allowed to swell for 24 h. Drug loaded hydrogel was washed 5 times to remove drug at the surface, and then placed in 10 mL pH 7.4 PBS. Drug release was performed at 37 °C in a water bath shaker at 80 rpm. At predetermined time points, all the release medium was removed, and replaced with the same volume of medium. The content of DOX in the release medium was determined by using a microplate reader at 490 nm (Spark®, Tecan).

2.8. In vitro anticancer activity

Sulforhodamine B (SRB) assay was used to evaluate the effect of free drug and drug-loaded hydrogels on proliferation of human breast cancer SK-BR-3 cell line (ATCC, HTB-30). 5 mg DOX was dissolved in 1 mL PBS. 50 mg dried gel was then added to the solution, and allowed to swell overnight to yield a drug-loaded hydrogel which was then freeze dried for 48 h. A weighed piece of drug-loaded hydrogel was used to determine the drug content. Cell suspension was prepared at a density of 5×10^4 cells/mL in McCoy's 5A culture medium supplemented with 10% FBS, 100 U/mL penicillin, 100 μg/mL streptomycin and 10 mM HEPES (pH 7.3). 1.0 mL suspension of SK-BR-3 cells was added to each well of a 24-well plate, and incubated for 24 h at 37 °C in a humidified atmosphere containing 5% CO_2 to allow cell adhesion. The culture medium was then removed, and transwell inserts with a polycarbonate porous membrane (0.4 μm pore size), containing gel samples, were placed in wells. Subsequently, culture medium was added at both sides of membrane and cell incubation then proceeded for 72. Cell incubation then proceeded for 72 h. Untreated cells were used as negative control.

At the end of the incubation period, the medium was withdrawn. The cells were fixed with 10% trichloroacetic acid for 1 h at 4 °C, washed three times with deionized water, dried completely under laminar flow cabinet, and finally stained with 0.4% sulforhodamine B solution (dissolved in 1% acetic acid). Unincorporated dye was removed by three times rinsing using 1.0% acetic acid, and incorporated dye was solubilized in 10 mM Tris base solution. Absorbance was measured at 570 nm and 690 nm (background absorbance) using MRX Revelation plate reader (Dynex Technologies). All experiments were realized in triplicate. For statistical analysis of the results One-way ANOVA was used.

3. Results and discussion

3.1. Characterization of copolymers and photo-initiator

Two series of PTMC-PEG-PTMC triblock copolymers were synthesized by ring-opening polymerization of TMC, using dihydroxyl terminated PEG with M_n of 6 K or 10 K g/mol as macro-initiator and stannous octoate as catalyst. The theoretical degree of polymerization (DP) of both PTMC blocks was 20 and 30, respectively. A typical ^{1}H NMR spectrum of PTMC-PEG-PTMC copolymers is shown in Fig. S1. The DP of TMC moieties was calculated from the integrations of the methylene protons of TMC and ethylene oxide repeating units. The obtained DP values are 17 and 27 for the PEK6K series, and 18 and 32 for the PEG10K series, which are very close to theoretical data as shown in Table 1. The triblock copolymers are named as PEG_x-$PTMC_y$, which x refers to the M_n of the PEG block and y to the total Mn of both PTMC blocks. The M_n of copolymers is 7730 and 8750 g/mol for the PEK6K series, and 11,840 and 13,260 g/mol for the PEG10K series.

Fig. 1 shows the NMR spectrum of acrylate functionalized PEG_{10k}-$PTMC_{1.8k}$-DA. Signal **a** at 3.66 ppm is attributed to the CH_2 protons of PEG main chain. Signals **b** and **c** at 2.05 and 4.24 ppm belong to the central and lateral methylene groups of PTMC. Three small signals detected at 5.60–6.30 ppm are assigned to the acryloyl group. The degree of substitution (DS) of the acryloyl group at both ends of copolymer chains was calculated from the integrations of end acrylate protons and methylene protons of ethylene oxide moieties.

The DS of PEG-PTMC-DA ranged from 50.0 to 65.1%, indicating successful acrylation of the hydroxyl endgroups (Table 1). The DS value of PEG_{10k}-DA is 50.0% which is lower than that of PEG_{6k}-DA (54.6%) due to the reactivity difference of terminal hydroxyl groups. The same trend is observed for the two groups of copolymers with similar PTMC block lengths as the DS values of PEG6K based copolymers are higher than those of PEG10K based copolymers. On the other hand, the DS values of the copolymers are higher than those of PEG-DA for both series. Apparently the reactivity of terminal hydroxyl groups could be slightly enhanced with attachment of PTMC blocks. Similar findings have been reported in the case of PCL-PEG-PCL copolymers. Xu et al. obtained DS values of 55, 59, and 60% for PEG_{20k}-DA, PEG_{20k}–PCL_{22k}-DA, and PEG_{20k}–PCL_{24k}-DA, respectively (Xu et al., 2018).

The molecular weight and dispersity (*Đ*) of the copolymers were also determined by GPC. As shown in Table 1, the Mn_{GPC} varies from 4840 to 8910, *i.e.* lower than the Mn values obtained from NMR. This difference could be attributed to the fact that the Mn_{GPC} was determined on the basis of hydrodynamic volume of copolymers in the eluent with respect to polystyrene standards. The dispersity of the copolymers ranges from 1.22 to 1.60, in agreement with a narrow distribution of molecular weights.

The hydrophilic-lipophilic balance (HLB) is a key parameter of amphiphilic copolymers. It was calculated according to Griffin's method (Huang et al., 2009; Zamani and Khoee, 2012; Sun et al., 2018).

$$HLB_{copolmer} = \frac{W_{PEG}}{W_{copolymer}} \times 20 \quad (5)$$

where $W_{PEG}/W_{Copolymer}$ is weight ratio of the hydrophilic PEG block to the whole copolymer. In general, copolymers with high hydrophobicity have an HLB value that tends to zero, and copolymers with high hydrophilicity have an HLB value close to 20. All copolymers present an HLB value ranging from 13.7 to 16.9 as shown in Table 1. The HLB value strongly affects the dissolving behavior. PEG_{10k}-$PTMC_{1.8k}$-DA copolymer with an HLB of 16.9 is quickly dissolved, and the solution appears totally transparent. In contrast, the dissolution process of PEG_{6k}-$PTMC_{2.7k}$-DA copolymer with an HLB of 13.7 is long and requires stirring. These findings are consistent with the literature data (Sharifi et al., 2012).

All the triblock copolymers and PEG-DA are semi-crystalline polymers. PEG_{6k}-DA exhibits a T_m at 57.1 °C with a melting enthalpy (ΔH_m) of 164.7 J/g. The T_m decreases to at 52.5 and 52.3 °C, and the ΔH_m to 108.4 and 76.9 J/g for PEG_{6k}-$PTMC_{1.7k}$-DA and PEG_{6k}-$PTMC_{2.7k}$-DA, respectively. The longer the PTMC block, the lower the T_m and ΔH_m values. In fact, attachment of PTMC blocks disfavors the crystallization of the central PEG block and thus leads to lower T_m and ΔH_m. Similar findings are obtained for PEG_{10k}-DA and corresponding copolymers. The DSC data are summarized in Table 1.

Table 1
Characterization of PEG-DA and PEG-PTMC-DA copolymers and hydrogels.

Copolymer	DP_{PEG}	DP_{PTMC}	Mn_{NMR} (g/mol)	DS (%)	Mn_{GPC} (g/mol)	Đ	HLB	T_m (°C)	Hm (J/g)	Swelling (%)	Weight loss (%)
PEG_{6k}-DA	136	–	–	54.6	–	–	–	57.1	164.7	2490 ± 180	29.7 ± 1.0
PEG_{6k}-$PTMC_{1.7k}$-DA	136	17 (20)	7730	61.4	4840	1.28	15.5	52.5	108.4	1780 ± 90	23.7 ± 2.7
PEG_{6k}-$PTMC_{2.7k}$-DA	136	27 (30)	8750	65.1	5770	1.60	13.7	52.3	76.9	1340 ± 50	11.6 ± 4.1
PEG_{10k}-DA	227	–	–	50.0	–	–	–	62.5	184.2	5880 ± 250	38.6 ± 1.5
PEG_{10k}-$PTMC_{1.8k}$-DA	227	18 (20)	11,840	56.0	8370	1.43	16.9	56.4	132.5	2470 ± 80	29.4 ± 6.0
PEG_{10k}-$PTMC_{3.2k}$-DA	227	32 (30)	13,260	58.0	8910	1.22	15.1	55.9	105.8	1620 ± 220	13.9 ± 8.0

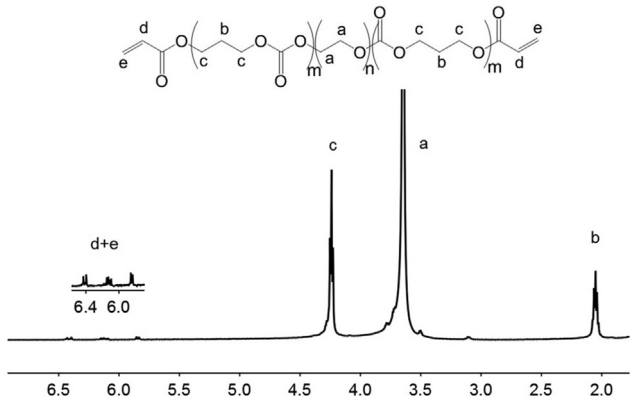

Fig. 1. ^{1}H NMR spectrum of PEG_{6k}-$PTMC_{2.7K}$-DA copolymer in $CDCl_3$.

As a water soluble photo-initiator, LAP was synthesized in a two-step process as previously described in literature (Majima et al., 1991). Dimethyl phenylphosphonite first reacted with 2,4,6-trimethylbenzoyl chloride via Michaelis-Arbuzov reaction, followed by reaction with lithium bromide to yield LAP. Fig. 2 shows the ^{1}H NMR spectrum of LAP in D_2O. The signals at 1.96 (a, 6H), 2.18 (b, 3H), 6.83 (c, 2H), 7.42 (d, 2H), 7.51 (e, 1H), and 7.66 (f, 2H) demonstrated the successful synthesis of the photo-initiator with expected chemical structure. The yield of the reaction was nearly 100%.

3.2. Preparation and characterization of hydrogels

PEG-PTMC-DA and PEG-DA hydrogels were formed by photo-crosslinking via visible-light initiation using LAP as water-soluble initiator. Fig. 3 schematically illustrates the formation of PEG-PTMC-DA hydrogels. Both LAP and PEG-PTMC-DA are dissolved in water. As the triblock copolymer has functional acrylate groups

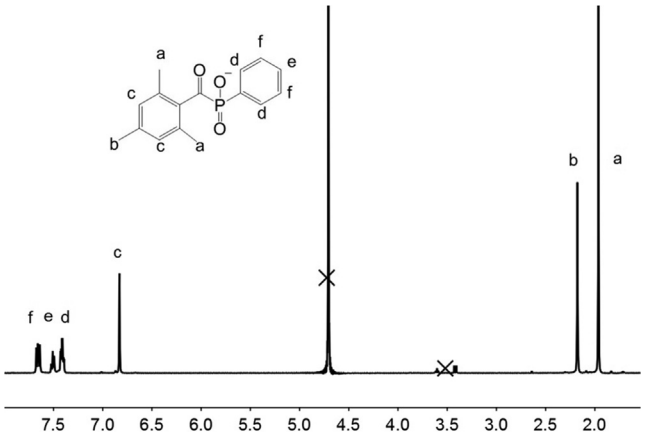

Fig. 2. ^{1}H NMR spectrum of LAP in D_2O.

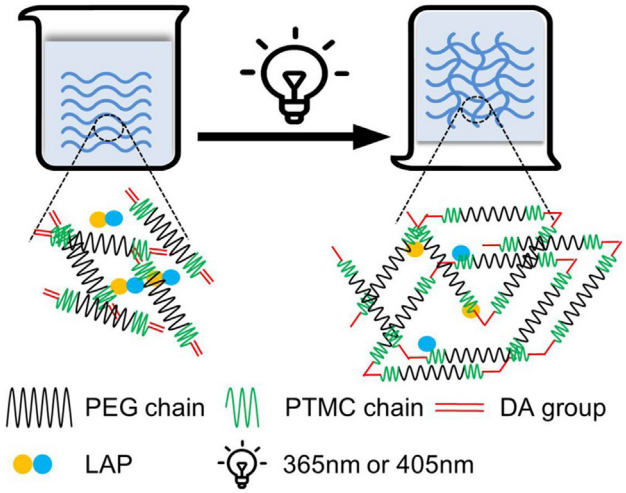

Fig. 3. Schematic illustration of the formation of PEG-PTMC-DA hydrogel network by photo-crosslinking via visible light irradiation using LAP as photo-initiator.

at both chain ends, the double bonds of acrylate are opened in the presence of LAP under irradiation of visible light, thereby coupling the copolymer chains to form a hydrogel network. It is noteworthy that diblock copolymers with only one acrylate chain end cannot form a network.

The formed PEG_{6k}-DA and PEG_{10k}-DA hydrogels were soft and transparent, and could be easily injected through an 18G syringe. PEG_{6k}-$PTMC_{1.7k}$-DA and PEG_{10k}-$PTMC_{1.8k}$-DA hydrogels with short PTMC blocks appeared whitish and slightly elastic, and could be injected through an 18G syringe (Fig. S2). In the case of PEG_{6k}-$PTMC_{2.7k}$-DA and PEG_{10k}-$PTMC_{3.2k}$-DA hydrogels with long PTMC blocks, they appeared whitish and highly elastic, and could be hardly injected through an 18G syringe. LAP was selected as photo-initiator because of its outstanding biocompatibility and water solubility. Moreover, cross-linking using visible light is much safer as compared to commonly used UV cross-linking (405 nm), and is thus most beneficial for medical applications.

The swelling properties of the various hydrogels were investigated by soaking as-obtained hydrogels in PBS for 48 h. PEG_{6k}-DA hydrogel exhibits a swelling ratio of 2490%, as shown in Table 1. With attachment of PTMC block, the swelling ratio decreases to 1780 and 1340% for PEG_{6k}-$PTMC_{1.7k}$-DA and PEG_{6k}-$PTMC_{2.7k}$-DA hydrogels, respectively. The higher the PTMC block length, the lower the degree of swelling. In the case of the PEG10K based hydrogels, PEG_{10k}-DA hydrogel exhibits a swelling ratio of 5780%, which is much higher than that of PEG_{6k}-DA hydrogel. This difference could be assigned to the lower Mn and higher DS of acrylated PEG_{6k}-DA as compared to PEG_{10k}-DA which lead to higher crosslinking density, and thus to lower swelling of PEG_{6k}-DA hydrogel. Attachment of PTMC block also leads to lower swelling degree as in the case of PEG_{6k} based hydrogels (Table 1). Thus the degree of swelling can be tailored by varying the M_n of PEG and the PTMC block length to meet the requirements of various applications.

On the other hand, the degree of weight loss was determined as non-crosslinked species were removed during swelling. PEG_{6k}-DA hydrogel exhibits a weight loss of 29.7% (Table 1), whereas the weight loss of PEG_{6k}-$PTMC_{1.7k}$-DA and PEG_{6k}-$PTMC_{2.7k}$-DA is 23.7 and 11.6%, respectively. The higher the PTMC block length, the lower the degree of weight loss. In the case of the PEG10K based hydrogels, PEG_{10k}-DA hydrogel exhibits a weight loss of 38.6%, which is higher than that of PEG_{6k}-DA hydrogel. This difference could be to the lower DS of acrylated PEG_{10k}-DA as compared to PEG_{6k}-DA as shown in Table 1. Lower DS leads to less crosslinking density, and thus to higher weight loss. On the other hand, the degree of weight loss decreases with increase in the PTMC block length of the copolymers. Therefore, the weight loss of hydrogels during swelling mainly depends on the DS or crosslinking density, and on the hydrophobic block length of copolymers.

The morphology of freeze dried hydrogels was examined by SEM microscopy. The images of PEG_{10K} based hydrogels are shown in Fig. 4. All hydrogels exhibit a highly porous structure. The pore size varies approximately from 20 to 100 μm. The wall surface of dried gels appears rather rough with folds for PEG_{10k}-$PTMC_{3.2k}$-DA (Fig. 4A) and PEG_{10k}-$PTMC_{1.8k}$-DA (Fig. 4B). In contrast, PEG_{10k}-DA seems to have a smooth surface (Fig. 4C). This difference could be attributed to the amphiphilic nature of the copolymers. Also, the wall of PEG_{10k}-DA appears thinner than that of PEG_{10k}-$PTMC_{3.2k}$-DA and PEG_{10k}-$PTMC_{1.8k}$-DA, in agreement with higher swelling of the former. Similar finding are obtained for PEG_{6K} based hydrogels (Fig S3).

3.3. Biocompatibility of hydrogels

3.3.1. MTT assay

MTT assay is used to evaluate the cytotoxicity of biomaterials *in vitro*, using L929 cell line. Fig. 5 shows the morphology of cells after 72 h co-culture with extracts of PEG_{6k}-$PTMC_{1.7k}$-DA and PEG_{10k}-$PTMC_{1.8k}$-DA freeze dried hydrogels in comparison with the negative and positive controls. Typically fibroblasts exhibit a fusiform or flat polygonal structure with clear cell contour. This is the case of cells after co-culture with the hydrogel extracts and the negative control, as shown in Fig. 5A, B, and C. Cells co-cultured with 0.05% phenol are round in shape and smaller in number (Fig. 5D). Cell morphology observation shows that both hydrogels have no adverse effects on cell growth.

Fig. 6 presents the cell viability data after culture in extracts of hydrogels for 24, 48 and 72 h. The RGR value of the positive control

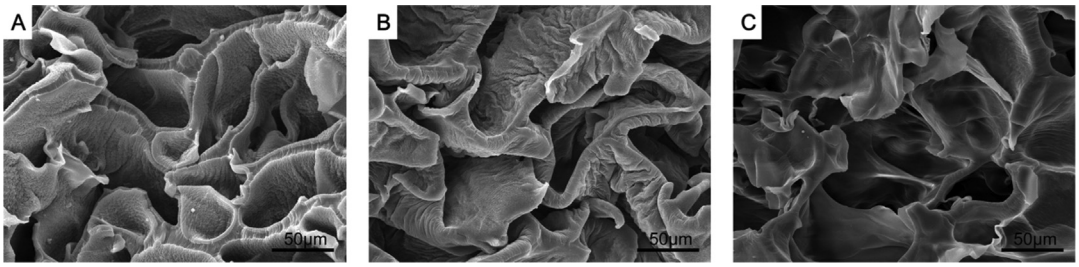

Fig. 4. SEM images of PEG_{10k}-$PTMC_{3.2k}$-DA (A), PEG_{10k}-$PTMC_{1.8k}$-DA (B) and PEG_{10k}-DA hydrogel (C).

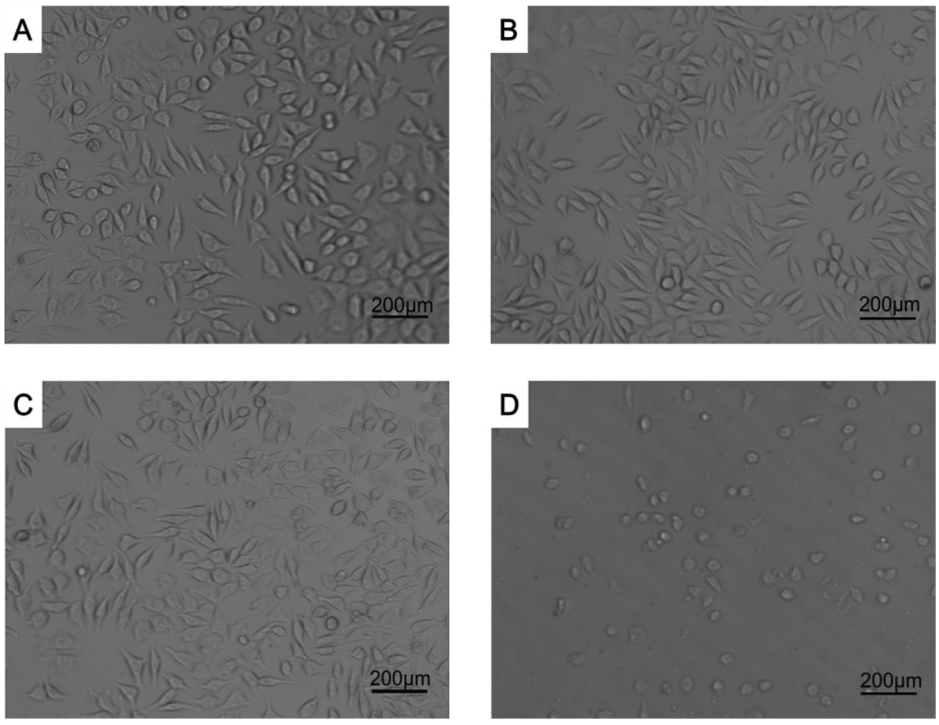

Fig. 5. Morphological observation of L929 cells after 72 h co-culturing with extracts of PEG_{6k}-$PTMC_{1.7k}$-DA (A), PEG_{10k}-$PTMC_{1.8k}$-DA (B) as compared to negative control (C) and positive control (D).

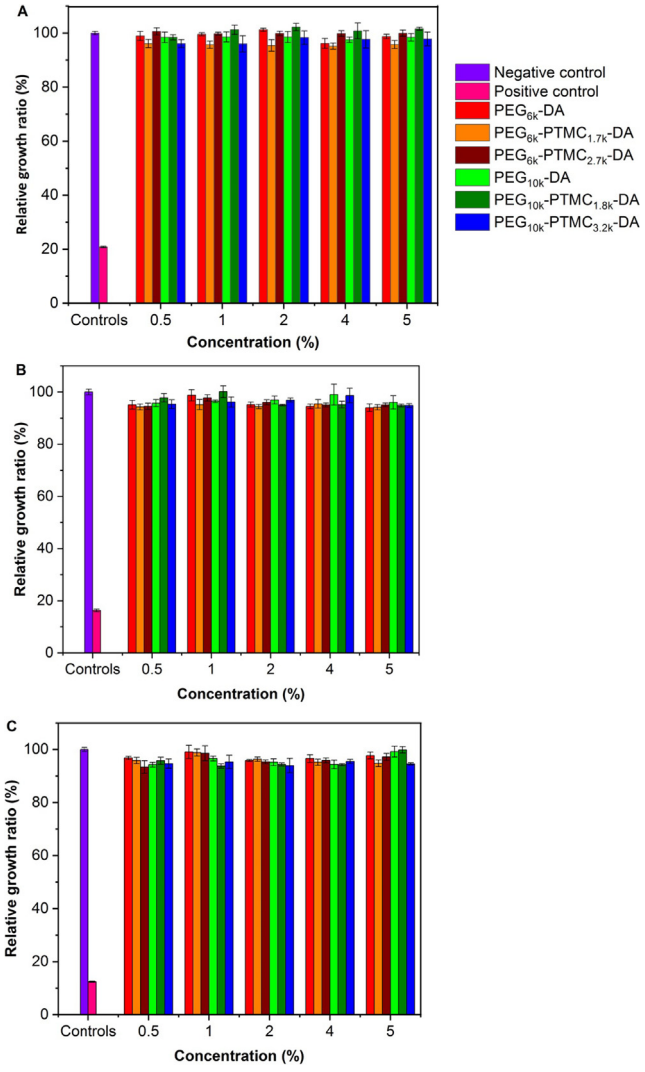

Fig. 6. Relative growth ratio of L929 cells after 24 h (A), 48 h (B) and 72 h (C) incubation with extracts of hydrogels at different concentrations compared to negative and positive controls.

is 12% which is quite low compared to the negative control (100%). In contrast, the RGR ranges from 93% to 102% for all PEG-PTMC-DA and PEG-DA hydrogel extracts at different concentrations. It is noteworthy that even at the longest incubation time, all the RGR values are above 93%. Thus the cytotoxicity levels are 0 or 1 for all hydrogel extracts. According to the United States Pharmacopeia Standards, it is concluded that PEG-PTMC-DA and PEG-DA hydrogels are not toxic to L929 cells; and can be used as potential biomedical materials.

3.3.2. Hemolysis test

Hemolysis test is widely used as a screening method of biomaterials as it allows to detect the breaking open of red blood cells (RBC) in contact with a material. Broken RBC will release hemoglobin into the blood that could lead to deformation of platelets and coagulation in vivo. Hemolysis ratio (HR) is used to quantify the degree of damaged RBC.

Table 2 lists the OD values and hemolysis ratios of PEG-PTMC-DA and PEG-DA hydrogels. The values of the negative and positive controls are within the range recommended by the Standard ISO 10993-4. In general, HR values below 5% are acceptable for biomedical applications. This is the case of all the hydrogel samples whose HR values are in the range from 1.62 to 2.56%.

Table 2
Hemolysis ratios of extracts of PEG-DA and PEG-PTMC-DA hydrogels.

Sample	OD value	Hemolysis ratio (%)
Saline	0.027 ± 0.007	Negative control
H_2O	0.77 ± 0.016	Positive control
PEG_{6k}-DA	0.046 ± 0.005	2.56 ± 0.67
PEG_{6k}-$PTMC_{1.7k}$-DA	0.046 ± 0.003	2.56 ± 0.40
PEG_{6k}-$PTMC_{2.7k}$-DA	0.045 ± 0.006	2.42 ± 0.81
PEG_{10k}-DA	0.045 ± 0.008	2.42 ± 0.11
PEG_{10k}-$PTMC_{1.8k}$-DA	0.039 ± 0.005	1.62 ± 0.67
PEG_{10k}-$PTMC_{3.2k}$-DA	0.044 ± 0.002	2.29 ± 0.27

3.3.3. Dynamic clotting time

Dynamic clotting time was used to assess the degree of activated endogenous clotting factors and the effect of hydrogels on clotting time when they are in contact with blood.

Fig. 7 illustrates the absorbance changes of hydrogel extracts compared to the positive and negative controls. The time at which the absorbance reaches 0.01 and 0.1 is generally defined as the whole clotting time and the initial blood setting time. The positive control exhibited the lowest absorbance throughout the test period up to 140 min. All the test samples showed the same trend, and the absorbance gradually decreased with time. The negative control exhibited slightly higher absorbance than the test samples until 100 min. The initial blood setting time of PEG-PTMC-DA and PEG-DA hydrogels varies from 50 to 60 min which is close to that of the negative control (70 min), but significantly longer than that of the positive control (18 min). Meanwhile, the whole clotting time of hydrogels and controls is at the same level (180 min). The dynamic clotting time tests illustrated that the extracts of hydrogels did not interplay with fibrinogen in blood, in agreement with outstanding anti-coagulant properties

3.4. In vitro drug release

DOX loading in PEG-PTMC-DA and PEG-DA hydrogels was realized by soaking dried gels in a DOX solution at 5.0 mg/mL. The drug loading efficiency was determined from the total amounts of released drug and residual drug in the gels to that of the initially added drug. Fig. 8 shows the drug loading efficiency of the 6 hydrogels. PEG_{6k}-DA hydrogel presents a drug loading of 70.0%. With the attachment of PTMC blocks, the drug loading decreased to 64.0% and 51.6% for PEG_{6k}-$PTMC_{1.7k}$-DA and PEG_{6k}-$PTMC_{2.7k}$-DA, respectively. Apparently, the drug loading capacity is closely related to

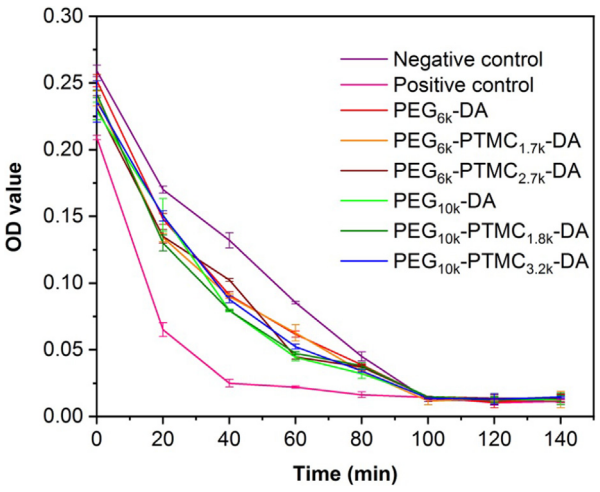

Fig. 7. OD value changes of hydrogel extracts as a function of time in comparison with the controls.

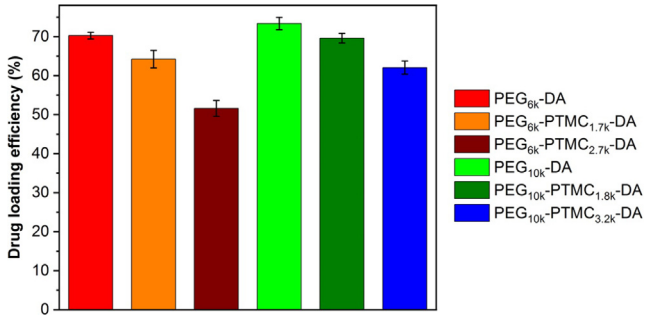

Fig. 8. Drug loading efficiency of PEG-PTMC-DA and PEG-DA hydrogels.

the swelling degree of hydrogels. Higher swelling degree of hydrogels leads to higher drug loading as they can absorb more drug solution. In the case of PEG_{10k} based hydrogels, PEG_{10k}-DA presents a drug loading of 73.4% which is higher than that of PEG_{6k}-DA. Attachment of PTMC blocks also leads to decrease of drug loading, in agreement with lower swelling degree.

Fig. 9 shows the cumulative drug release presents of all the drug loaded hydrogels as a function of time. Two stages are clearly distinguished. A strong burst is observed during the first 24 h, followed by slower release up to 15 days. PEG_{10k}-DA hydrogel presents the highest release ratio during the whole release period. An initial burst of 82% at 24 h and almost complete release of 97.5% at 15 days are detected. PEG_{6k}-$PTMC_{2.7k}$-DA exhibits the slowest release rate with an initial burst of 69.8% and a final release of 80.6%. Intermediate drug release rates are observed for the other hydrogels. Apparently the drug release rate is strongly related to the swelling ratio. Higher swelling leads to faster drug release. In fact, the drug release mechanism of hydrogel mainly depends on drug diffusion and degradation or disintegration of hydrogel network. In this work, drug diffusion is the main release mechanism as no degradation of hydrogels is observed during the release period. In fact, PTMC hardly undergoes hydrolytic degradation in the absence of enzymes (Yang et al., 2010). The amounts of released drug from the various hydrogels are shown in Fig. S4 and S5, taking into account the different drug loading contents. The same trend is observed as that shown in Fig. 9.

3.5. In vitro anticancer activity

PEG_{6k}-$PTMC_{1.7k}$-DA and PEG_{10k}-$PTMC_{1.8k}$-DA hydrogels with short PTMC blocks are easily injectable through a syringe. They were selected to evaluate the effect of drug loaded hydrogels on proliferation of SK-BR-3 tumor cells by SRB assay. Blank hydrogels were investigated at weights of 0.5, 1.0 and 2.0 mg which correspond to those of drug loaded hydrogels. Proliferation of cells cultured with blank hydrogels was comparable with that of the control. Even the highest concentration of PEG-PTMC-DA hydrogel had no negative effect on the growth of SK-BR-3 cells that is shown

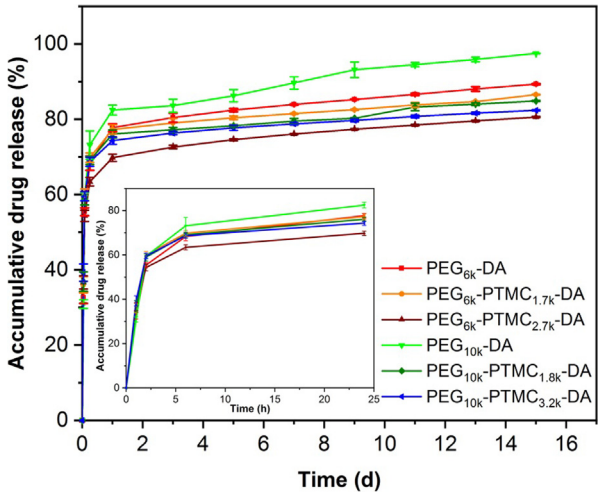

Fig. 9. Drug release profiles of DOX-loaded PEG-PTMC-DA and PEG-DA hydrogels.

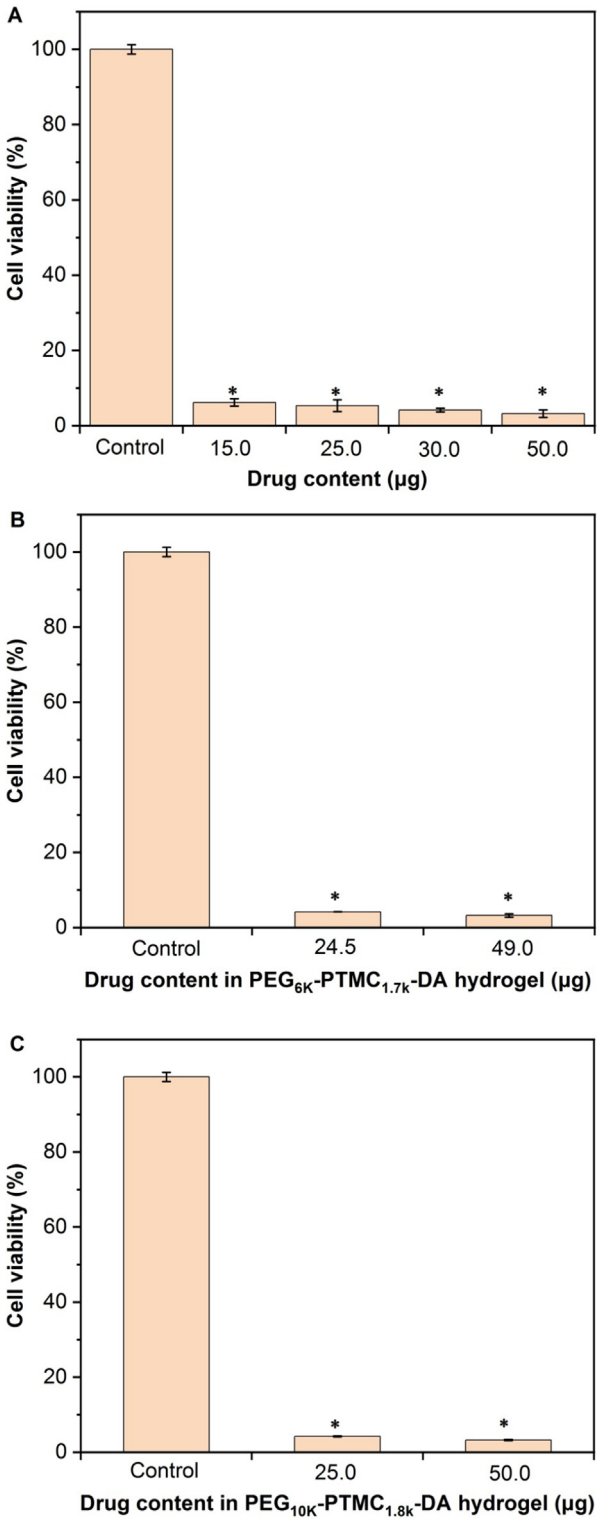

Fig. 10. Effect of free doxorubicin (A) and doxorubicin loaded in PEG_{6k}-$PTMC_{1.7k}$-DA (B) and PEG_{10k}-$PTMC_{1.8k}$-DA (C) loaded hydrogel on proliferation of SK-BR-3 cells ($P < 0.05$ versus the control group).

in Fig. S6, in agreement with the results obtained by MTT assay on murine fibroblasts (Fig. 6).

The proliferation of SK-BR-3 cells was analyzed in the presence of various amounts of free drug in a range of 15.0–50.0 μg, and drug loaded PEG_{6k}-$PTMC_{1.7k}$-DA and PEG_{10k}-$PTMC_{1.8k}$-DA hydrogels. The initial drug loading of PEG_{6k}-$PTMC_{1.7k}$-DA and PEG_{10k}-$PTMC_{1.8k}$-DA hydrogels was 62 and 65 μg/mg, and the amounts of hydrogel added to each well were 0.5 and 1.0 mg, respectively. Taking into account the cumulative drug release of 79% and 77% during the first 3 days (Fig. 9), the drug weight in PEG_{6k}-$PTMC_{1.7k}$-DA and PEG_{10k}-$PTMC_{1.8k}$-DA hydrogels was estimated 24.5 and 49.0, and 25.0 and 50.0 μg in each well, respectively. As shown in Fig. 10, free DOX at different concentrations and drug loaded hydrogels significantly reduced SK-BR-3 tumor cell proliferation compared to the untreated cells (Control). Viability of cells decreased from 6.16 to 3.20% with increasing free drug content from 15.0 to 50.0 μg. Similarly, significant cytotoxicity of drug loaded hydrogels was observed (decrease of cell viability from 4.17 to 3.20%, and from 4.21 to 3.23% with increasing drug content from 24.5 to 49.0 μg, and from 25.0 to 50.0 μg for DOX loaded PEG_{6k}-$PTMC_{1.7k}$-DA and PEG_{10k}-$PTMC_{1.8k}$-DA hydrogels, respectively). Therefore, drug loaded hydrogels exhibit comparable cytotoxic effect on SK-BR-3 tumor cells with free drug.

4. Conclusion

In this study, in situ forming hydrogels were prepared by photo-crosslinking diacrylated PEG-PTMC-DA and PEG-DA copolymers using LAP as photo-initiator, and characterized. The degree of swelling and weight loss of hydrogels are dependent on the degree of substitution of chain ends and PTMC block length. Higher degree of substitution and longer PTMC block length lead to lower degree of swelling and weight loss. Meanwhile, freeze dried hydrogels exhibit a highly porous structure with pore size approximately ranging from 20 to 100 μm. MTT assay, hemolysis test, and dynamic clotting time measurements show that the hydrogels present outstanding cyto- and hemocompatibility. Finally, drug loading and drug release behaviors of the hydrogels with various compositions were investigated using DOX as a hydrophilic model drug. And the effect of drug loaded hydrogels on SK-BR-3 tumor cells was evaluated in comparison with free drug. Similar cytotoxicity was obtained for drug loaded hydrogels and free drug at comparable drug concentrations. It is thus concluded that injectable PEG-PTMC-DA hydrogels could be a promising bioresorbable carrier of hydrophilic drugs.

Declaration of Competing Interest

The authors declared that there is no conflict of interest.

Acknowledgment

The work was financially supported by the Science and Technology Development Plan of Shandong Province (2018GGX102016) and the 2018 Shandong Province Graduate Education Joint Training Base Construction Project. The research was supported by the Programme—International scholarship exchange of PhD candidates and academic staff, organized by Medical University of Silesia in Katowice.

Appendix A. Supplementary material

Supplementary data to this article can be found online at https://doi.org/10.1016/j.jsps.2020.01.008.

References

Altieri, P., Barisione, C., Lazzarini, E., Garuti, A., Bezante, G., Canepa, M., Spallarossa, P., Tocchetti, C., Bollini, S., Brunelli, C., Ameri, P., 2016. Testosterone antagonizes doxorubicin-induced senescence of cardiomyocytes. J. Am. Heart Assoc. 5, e002383. https://doi.org/10.1161/JAHA.115.002383.

Bastiancich, C., Bozzato, E., Luyten, U., Danhier, F., Bastiat, G., Préat, V., 2019. Drug combination using an injectable nanomedicine hydrogel for glioblastoma treatment. Int. J. Pharm. 559, 220–227. https://doi.org/10.1016/j.ijpharm.2019.01.042.

Bhosle, J., Hall, G., 2009. Principles of cancer treatment by chemotherapy. Surgery (Oxford) 27 (4), 173–177. https://doi.org/10.1016/j.mpsur.2009.01.006.

Brunelle, A.R., Horner, C.B., Low, K., Ico, G., Nam, J., 2018. Electrospun thermosensitive hydrogel scaffold for enhanced chondrogenesis of human mesenchymal stem cells. Acta Biomater. 66, 166–176. https://doi.org/10.1016/j.actbio.2017.11.020.

Buchtova, N., D'orlando, A., Judeinstein, P., Chauvet, O., Weiss, P., Le Bideau, J., 2018. Water dynamics in silanized hydroxypropyl methylcellulose based hydrogels designed for tissue engineering. Carbohy. Polym. 202, 404–408. https://doi.org/10.1016/j.carbpol.2018.08.143.

Cheng, Y., Zou, T., Dai, M., He, X.Y., Peng, N., Wu, K., Wang, X.Q., Liao, C.Y., Liu, Y., 2019. Doxorubicin loaded tumor-triggered targeting ammonium bicarbonate liposomes for tumor-specific drug delivery. Colloid. Surface. B 178, 263–268. https://doi.org/10.1016/j.colsurfb.2019.03.002.

Dong, J.T., Liao, L., Ma, Y., Shi, L., Wang, G.X., Fan, Z.Y., Li, S.M., Lu, Z.Q., 2014. Enzyme-catalyzed degradation behavior of L-lactide/trimethylene carbonate/glycolide terpolymers and their composites with poly(L-lactide-co-glycolide) fibers. Polym. Degrad. Stabil. 103, 26–34. https://doi.org/10.1016/j.polymdegradstab.2014.03.004.

Echave, M.C., Pimenta-Lopes, C., Pedraz, J.L., Mehrali, M., Dolatshahi-Pirouz, A., Ventura, F., Orive, G., 2019. Enzymatic crosslinked gelatin 3D scaffolds for bone tissue engineering. Int. J. Pharm. 562, 151–161. https://doi.org/10.1016/j.ijpharm.2019.02.043.

Fairbanks, B.D., Schwartz, M.P., Bowman, C.N., Anseth, K.S., 2009. Photoinitiated polymerization of PEG-diacrylate with lithium phenyl-2, 4, 6-trimethylbenzoylphosphinate: polymerization rate and cytocompatibility. Biomaterials 30 (35), 6702–6707. https://doi.org/10.1016/j.biomaterials.2009.08.055.

Hamedi, H., Moradi, S., Hudson, S.M., Tonelli, A.E., 2018. Chitosan based hydrogels and their applications for drug delivery in wound dressings: a review. Carbohyd. Polym. 199, 445–460. https://doi.org/10.1016/j.carbpol.2018.06.114.

Huang, M.H., Huang, C.Y., Lien, S.P., Siao, S.Y., Chou, A.H., Shen, H.W., Liu, S.J., Leng, C.H., Chong, P., 2009. Development of multi-phase emulsions based on bioresorbable polymers and oily adjuvant. Pharm. Res. 26 (8), 1856–1862. https://doi.org/10.1007/s11095-009-9898-y.

Kavian, Z., Alavizadeh, S.H., Golmohamadzadeh, S., Badiee, A., Khamesipour, A., Jaafari, M.R., 2019. Development of topical liposomes containing miltefosine for the treatment of Leishmania major infection in susceptible BALB/c mice. Acta Trop. 196, 142–149. https://doi.org/10.1016/j.actatropica.2019.05.018.

Kim, H.S., Yang, J., Kim, K., Shin, U.S., 2019. Biodegradable and injectable hydrogels as an immunosuppressive drug delivery system. Mat. Sci. Eng. C-Mater 98, 472–481. https://doi.org/10.1016/j.msec.2018.11.051.

Koehler, J., Brandl, F.P., Goepferich, A.M., 2018. Hydrogel wound dressings for bioactive treatment of acute and chronic wounds. Eur. Polym. J. 100, 1–11. https://doi.org/10.1016/j.eurpolymj.2017.12.046.

Liu, X., Wang, Y.X., Yun, P., Shen, X., Su, F., Chen, Y.S., Li, S.M., Song, D.Q., 2018. Self-assembled filomicelles prepared from polylactide-poly (ethylene glycol) diblock copolymers for sustained delivery of cycloprotoberberine derivatives. Saudi Pharm. J. 26 (3), 342–348. https://doi.org/10.1016/j.jsps.2018.01.008.

Liyanage, P.Y., Hettiarachchi, S.D., Zhou, Y., Ouhtit, A., Seven, E.S., Oztan, C.Y., Celik, E., Leblanc, R.M., 2019. Nanoparticle-mediated targeted drug delivery for breast cancer treatment. BBA-Rev. Cancer 1871, 419–433. https://doi.org/10.1016/j.bbcan.2019.04.006.

Majima, T., Schnabel, W., Weber, W., 1991. Phenyl-2,4,6-trimethylbenzoylphosphinates as water-soluble photoinitiators. Generation and reactivity of $O=P(C_6H_5)(O^-)$ radical anions. Macromol. Chem. Phys. 192 (10), 2307–2315. https://doi.org/10.1002/macp.1991.021921010.

Oh, K.S., Hwang, C., Lee, H.Y., Song, J.S., Park, H.J., Lee, C.K., Song, I., Lim, T.H., 2019. Preclinical studies of ropivacaine extended-release from a temperature responsive hydrogel for prolonged relief of pain at the surgical wound. Int. J. Pharm. 558, 225–230. https://doi.org/10.1016/j.ijpharm.2019.01.011.

Pugazhendhi, A., Edison, T.N.J.I., Velmurugan, B.K., Jacob, J.A., Karuppusamy, I., 2018. Toxicity of Doxorubicin (Dox) to different experimental organ systems. Life Sci. 200, 26–30. https://doi.org/10.1016/j.lfs.2018.03.023.

Qureshi, M.A., Khatoon, F., 2019. Different types of smart nanogel for targeted delivery. J. Sci. Adv. Mat. Dev. 4 (2), 201–212. https://doi.org/10.1016/j.jsamd.2019.04.004.

Ross, A.E., Bengani, L.C., Tulsan, R., Maidana, D.E., Salvador-Culla, B., Kobashi, H., Kolovou, P.E., Zhai, H., Taghizadeh, K., Kuang, L., Mehta, M., Vavvas, D.G., Kohane, D.S., Ciolino, J., 2019. Topical sustained drug delivery to the retina with a drug-eluting contact lens. Biomaterials 119285. https://doi.org/10.1016/j.biomaterials.2019.119285.

Saberzadeh-Ardestani, B., Khosravi, B., Zebardast, J., Sadighi, S., 2019. Chemotherapy effect on daytime sleepiness and contributing factors in older adults with

cancer. J. Geriatr. Oncol. 10 (4), 632–636. https://doi.org/10.1016/j.jgo.2018.10.003.
Schneider, E.L., Henise, J., Reid, R., Ashley, G.W., Santi, D.V., 2016. Hydrogel drug delivery system using self-cleaving covalent linkers for once-a-week administration of exenatide. Bioconjugate Chem. 27 (5), 1210–1215. https://doi.org/10.1021/acs.bioconjchem.5b00690.
Sharifi, S., Kranenburg, H.J.C., Meij, B.P., Grijpma, D.W., 2011. Photo-crosslinkable poly (trimethylene carbonate)-based macromers for closure of ruptured intervertebral discs. Macromol. Symp. 309 (1), 100–110. https://doi.org/10.1002/masy.201100047.
Sharifi, S., Blanquer, S.B., van Kooten, T.G., Grijpma, D.W., 2012. Biodegradable nanocomposite hydrogel structures with enhanced mechanical properties prepared by photo-crosslinking solutions of poly (trimethylene carbonate)–poly (ethylene glycol)–poly (trimethylene carbonate) macromonomers and nanoclay particles. Acta Biomater. 8 (12), 4233–4243. https://doi.org/10.1016/j.actbio.2012.09.014.
Su, F., Yun, P., Li, C.L., Li, R.Y., Xi, L.S., Wang, Y.D., Chen, Y.S., Li, S.M., 2019. Novel self-assembled micelles of amphiphilic poly (2-ethyl-2-oxazoline)-poly (L-lactide) diblock copolymers for sustained drug delivery. Colloid. Surface. A 566, 120–127. https://doi.org/10.1016/j.colsurfa.2019.01.015.
Su, F., Wang, Y.D., Liu, X., Shen, X., Zhang, X.J., Xing, Q.S., Chen, Y.S., 2018. Biocompatibility and in vivo degradation of chitosan based hydrogels as potential drug carrier. J. Biomat. Sci., Polym. E. 29 (13), 1515–1528. https://doi.org/10.1080/09205063.2017.1412244.
Sun, X.K., Liu, X., Li, C.L., Wang, Y.D., Liu, L., Su, F., Li, S.M., 2018. Self-assembled micelles prepared from poly (ε-caprolactone)–poly (ethylene glycol) and poly (ε-caprolactone/glycolide)–poly (ethylene glycol) block copolymers for sustained drug delivery. J. Appl. Polym. Sci. 135 (9), 45732. https://doi.org/10.1002/app.45732.
Tomić, I., Juretić, M., Jug, M., Pepić, I., Čižmek, B.C., Filipović-Grčić, J., 2019. Preparation of in situ hydrogels loaded with azelaic acid nanocrystals and their dermal application performance study. Int. J. Pharm. 563, 249–258. https://doi.org/10.1016/j.ijpharm.2019.04.016.
Ullah, K., Sohail, M., Buabeid, M.A., Murtaza, G., Ullah, A., Rashid, H., Khan, M.A., Khan, S.A., 2019a. Pectin-based (LA-co-MAA) semi-IPNS as a potential biomaterial for colonic delivery of oxaliplatin. Int. J. Pharm. 569, 118557. https://doi.org/10.1016/j.ijpharm.2019.118557.
Ullah, K., Khan, S.A., Murtaza, G., Sohail, M., Manan, A., Afzal, A., 2019b. Gelatin-based hydrogels as potential biomaterials for colonic delivery of oxaliplatin. Int. J. Pharm. 556, 236–245. https://doi.org/10.1016/j.ijpharm.2018.12.020.
Wang, J., Cheng, Y., Fan, Z., Li, S., Liu, X., Shen, X., Su, F., 2016. Composites of poly (L-lactide-trimethylene carbonate-glycolide) and surface modified calcium carbonate whiskers as a potential bone substitute material. RSC Adv. 6 (62), 57762–57772. https://doi.org/10.1039/C6RA07832J.
Wang, J., Du, B., Fan, Z., Li, S., Yun, P., Su, F., 2018. Composites of poly (L-lactide-trimethylene carbonate-glycolide) and surface modified SBA-15 as bone repair material. Polym. Advan. Technol. 29 (4), 1322–1333. https://doi.org/10.1002/pat.4244.
Whitely, M., Cereceres, S., Dhavalikar, P., Salhadar, K., Wilems, T., Smith, B., Mikos, A., Cosgriff-Hernandez, E., 2018. Improved in situ seeding of 3D printed scaffolds using cell-releasing hydrogels. Biomaterials 185, 194–204. https://doi.org/10.1016/j.biomaterials.2018.09.027.
Wichterle, O., Lim, D., 1960. Hydrophilic gels for biological use. Nature 185 (4706), 117. https://doi.org/10.1038/185117a0.
Xi, L.S., Wang, Y.D., Su, F., Zhu, Q.Z., Li, S., 2019. Biocompatibility and degradation studies of poly (L-lactide-co-trimethylene carbonate) copolymers as cardiac occluders. Materialia 7, 100414. https://doi.org/10.1016/j.mtla.2019.100414.
Xu, C., Lee, W., Dai, G., Hong, Y., 2018. A highly elastic biodegradable single-network hydrogel for cell printing. ACS Appl. Mater. Interfaces 10, 9969–9979. https://doi.org/10.1021/acsami.8b01294.
Yang, L., Zhao, Z.X., Wei, J., Ghzaoui, A.E., Li, S.M., 2007. Micelles formed by self-assembling of polylactide/poly(ethylene glycol) block copolymers in aqueous solutions. J. Colloid Interf. Sci. 314 (2), 470–477. https://doi.org/10.1016/j.jcis.2007.05.074.
Yang, J., Liu, F., Yang, L., Li, S., 2010. Hydrolytic and enzymatic degradation of poly (trimethylene carbonate-co-D, L-Lactide) random copolymers with shape memory behavior. Eur. Polym. J. 46, 783–791. https://doi.org/10.1016/j.eurpolymj.2009.12.017.
Yang, Q.J., Yang, G.J., Wan, L.L., Han, Y.L., Huo, Y., Li, J., Huang, J.L., Lu, J., Gan, R., Guo, C., 2017. Protective effects of dexrazoxane against doxorubicin-induced cardiotoxicity: a metabolomic study. PloS One 12 (1). https://doi.org/10.1371/journal.pone.0169567.
Zamani, S., Khoee, S., 2012. Preparation of core–shell chitosan/PCL-PEG triblock copolymer nanoparticles with ABA and BAB morphologies: effect of intraparticle interactions on physicochemical properties. Polymer 53 (25), 5723–5736. https://doi.org/10.1016/j.polymer.2012.09.051.
Zhang, C., Aung, A., Liao, L., Varghese, S., 2009. A novel single precursor-based biodegradable hydrogel with enhanced mechanical properties. Soft Matter 5 (20), 3831–3834. https://doi.org/10.1039/B912102A.
Zhang, C., Sangaj, N., Hwang, Y., Phadke, A., Chang, C.W., Varghese, S., 2011. Oligo (trimethylene carbonate)–poly (ethylene glycol)–oligo (trimethylene carbonate) triblock-based hydrogels for cartilage tissue engineering. Acta biomater. 7 (9), 3362–3369. https://doi.org/10.1016/j.actbio.2011.05.024.
Zhang, E., Chen, H., Shen, F., 2010. Biocorrosion properties and blood and cell compatibility of pure iron as a biodegradable biomaterial. J. Materi. Sci., Mater M. 21 (7), 2151–2163. https://doi.org/10.1007/s10856-010-4070-0.
Zhang, W., Jin, X., Li, H., Zhang, R.R., Wu, C.W., 2018. Injectable and body temperature sensitive hydrogels based on chitosan and hyaluronic acid for pH sensitive drug release. Carbohyd. Polym. 186, 82–90. https://doi.org/10.1016/j.carbpol.2018.01.008.